



Effect of Microfins on Thermal Performance of Microchannel Using CFD

Wei Long Yeo^{1*}, Kim Ho Yeap¹, Koon Chun Lai¹, Pei Song Chee², Kok Seng Ong¹

¹Faculty of Engineering and Green Technology, Universiti Tunku Abdul Rahman, 31900 Kampar, Perak, Malaysia

²Lee Kong Chian Faculty of Engineering and Science, Universiti Tunku Abdul Rahman, 43000 Kajang, Selangor, Malaysia

*Corresponding author E-mail: weilong929@gmail.com

Abstract

In the present study, the fluid flow and heat transfer characteristic of microchannel heat sink with microfins are studied numerically at Reynold number ranging from 400 to 1200. The influence of microfins on the Nusselt number and pressure drop are investigated. Five different types of microfins namely cylindrical microfins (Case A), diverge cylindrical microfins (Case B), diverge cylindrical microfins with semi-circle rib (Case C), diverge cylindrical microfins with rectangular rib (Case D) and diverge cylindrical microfins with triangular rib (Case E) are designed. A comparative analysis of these five types of microfins with bare microchannel has been conducted. The result highlighted the extended microfins augmented the heat transfer characteristic by disrupt the thermal boundary layer. The overall thermal performances of microchannel heat sink with microfins are 1.1 – 1.47 times higher compared to bare microchannel.

Keywords: Extended surface; Heat transfer enhancement; Microchannel heat sink; Microfins.

1. Introduction

Since past decades, applications of miniaturization are immense in microelectronic industries, especially cooling of the high power light emitting diodes [1-2]. This however creates an issue to the effective thermal management when a large amount of heat is generated on the small surface area [3]. Different methods were proposed to meet the high heat flux requirements including the use of thermoelectric and vapor chamber [4-7].

Recently, the use of microchannel heat sink is drawing researchers' attention for dissipating high heat flux and cooling high power microelectronics owing to its higher efficient over the traditional heat sink [8]. Microchannel heat sink comprises a number of microchannels that ensure the laminar flow through the heat sink. Typically, the heat sink is attached to the substrates of electronic components. Attributing to the thinner thermal boundary layer induced by the microchannels, higher heat transfer rate can be thus achieved [9].

To date, microchannel heat sink has been widely employed on the heat spreader of the microprocessor [10-11]. In the efforts of enhancing the heat transfer performance, a large amount of researches have been carried out so as to investigate the nature of heat transfer, study the optimal configurations of heat sink and analyze the characteristics of microchannel with different shapes of ribs. In [12] reported that heat transfer performance can be improved with ribs in the microchannel. On the other hand, in [13] proposed the use of inline pin fins to entrench on microchannels. It was observed that the proposed device with pin fins have relative higher heat transfer coefficients than the plain microchannels. Likewise, in [14] examined the microchannels with ribs and fan-shaped reentrant. Their findings indicated that the heat transfer performance was improved compared to the microchannels with smooth surface.

Through numerical study, in [15] found the microchannel with wavy design generated higher flow rate. Besides, a study from [16] revealed that thermal resistance was reduced for microchannel with two-layer. It implies that heat dissipation rate is closely related to the flow contact area of the microchannel heat sink. In other words, microchannel with larger flow contact surface enhances the heat flow rate.

In search of the optimum heat transfer performance, in [17] numerically studied different rib positions and configurations (e.g. rectangular ribs and ellipsoidal ribs). They reported that there was an optimal length or width value provided the maximal improvement factor. Moreover, in [18] analyzed the effects of triangular, rectangular and semicircular ribs on the laminar flow via numerical simulation.

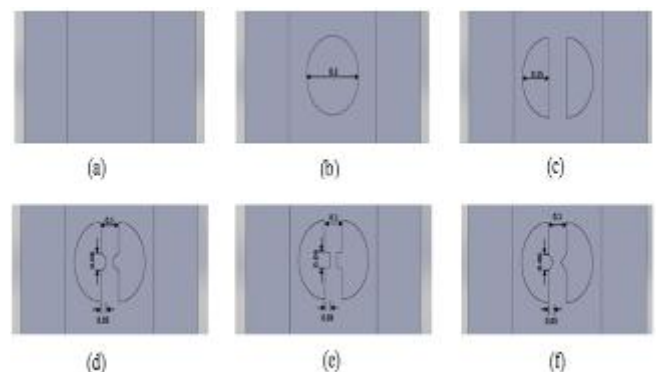


Fig. 1: Top views of the microchannel (dimension in mm): (a) Bare, (b) Case A, (c) Case B, (d) Case C, (e) Case D and (f) Case E

The results showed that rectangular ribs were inappropriate to be used compared to the semicircular ribs as the former design produced weaker laminar flow and heat transfer rate.

Though the use of ribs enhances the heat transfer performance, in fact it also results in considerable pressure drop penalty in microchannels. Hence, it is crucial to source for an efficient design to balance the heat transfer and pressure loss. In the present study, we propose a ribbed microchannel heat sink which enhances the heat transfer performance on one hand and reduces the pressure loss on the other hand. Numerical study was therefore carried out in order to elucidate the single phase heat transfer phenomena.

2. Materials and Methods

In this study, we compared several configurations of microchannel heat sink with microfins namely cylindrical microfins (Case A), diverge cylindrical microfins (Case B), diverge cylindrical microfins with semi-circle rib (Case C), diverge cylindrical microfins with rectangular rib (Case D) and diverge cylindrical microfins with triangular rib (Case E) with the bare rectangular microchannel. Figure 1 shows the schematic diagrams of the microchannel heat sink with different fin designs. The overall dimensions of the microchannel are $36 \times 0.5 \times 0.7 \text{ mm}^3$, the height of micro-fins is 0.4 mm and the fin-to-fin distance (pitch of fins) is set as 3 mm.

In this numerical study, single slice of microchannel was used for simulation instead of entire heat sink. The neighbouring solid surface and fluid flowing across it have been taken in account. The following assumptions were considered in order to simplify the simulation model [19]:

- Plain water as working fluid
- Steady flow, laminar, incompressible and Newtonian
- Radiation heat transfer is neglected
- Uniform heat flux throughout bottom wall

The inlet velocity, U_0 was ranging from 0.689 to 2.067 m/s and inlet temperature, T_0 was set to 295 K. The Reynolds number which defines the degree of laminar or turbulent flow is calculated by:

$$Re = \rho u d / \mu \quad (1)$$

where ρ denotes fluid density, u denotes fluid velocity and μ denotes dynamic fluid viscosity. The hydraulic diameter, d is expressed as:

$$d = \frac{4A}{P} = \frac{2WH}{W+H} \quad (2)$$

where A denotes the flow area and P represents the wetted parameter of microchannel. The commercial software of ANSYS Fluent 17.2 was employed for the numerical simulation. The SIMPLE method was adopted in the numerical study to determine the pressure-velocity coupling.

3. Results and Discussion

3.1. Validation of Model

Comparisons of our numerical simulation with experiment findings by [20-21] were firstly conducted in order to validate the proposed model in the present study. By adopting the same model, experiment results for the bare rectangular microchannel case was selected for comparison. Figure 2(a) shows the Nusselt number changed with different values of Reynolds number. Obviously, the simulated data in this study are in good agreement with the empirical findings of [20]. Whereas, Figure 2(b) shows another comparison of pressure drops with varied Reynolds number. Good agreement can again be seen.

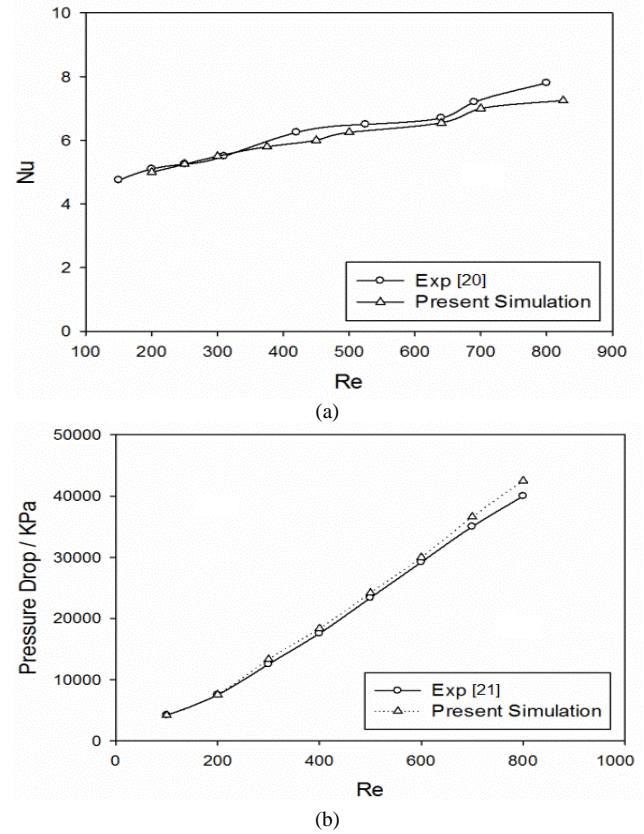


Fig. 2: Comparison of numerical result with experiment data: (a) Nusselt number and (b) Pressure drop

3.2. Velocity Distribution

Figure 3 illustrates the velocity distribution in the microchannel. As it can be seen in Figure 3(a), the maximum velocity located at the central portion of microchannel. The fast fluid flows at the middle portion promoted the continuous thickening of thermal boundary layer. Significant temperature difference between the central portion and channel wall led to the poor heat transfer performance. For Figure 3(b) and (c), the maximum velocity moved to both side of the wall after impinged with the cylindrical microfins. Although the appearances of cylindrical microfins helped to interrupt the thermal boundary layer, but it also created a laminar stagnation zone after the microfins. The fluid flowed so slow at the laminar stagnation zone declined the heat transfer rate.

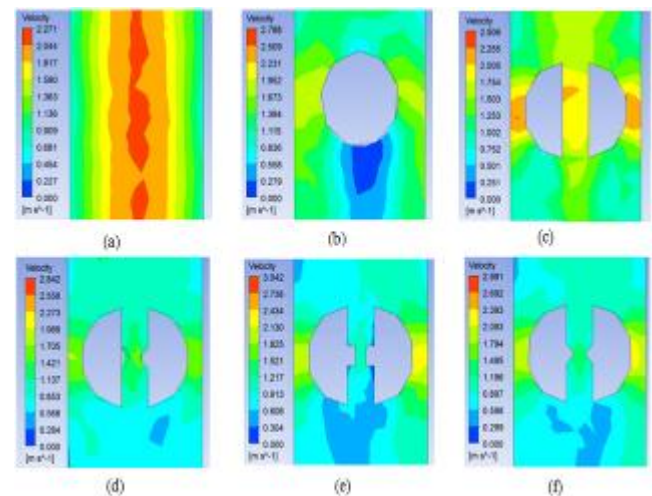


Fig. 3: Velocity distribution flow from top to bottom: (a) Bare, (b) Case A, (c) Case B, (d) Case C, (e) Case D and (f) Case E

As shown in Figure 3(d), (e) and (f), the laminar stagnation become lesser compared to Figure 3(b). This can be due to the deviation of the microfins, whereby the diverge part allowed the fluid to

pass through and the microribs disturbed the flow on the high velocity region. The velocity gradient represents the hot and cold fluid mixing level. A lesser velocity difference indicates a superior level of the mixing. From the observation, Case C has better flow distribution than other cases as the velocity gradient is smaller.

3.3. Temperature Distribution

Figure 4 depicts the relationship between the temperatures and the Reynolds number. It is apparent that the bare microchannel has the highest temperature compared to other designs of microchannel. This phenomenon is caused by the continuous thickening of thermal boundary layer along the straight microchannel. Besides, the average interface temperature of Case C was significantly reduced when compared to the bare rectangular microchannel. This can be accredited to the existence of microfins in the middle part of microchannel. The presence of extended surface helped to disrupt the temperature profile and prevented the thermal boundary layer achieved to fully developed state. Meanwhile, the microfins created redevelopment of thermal boundary layer and augmented the mixing of fluid at the side wall.

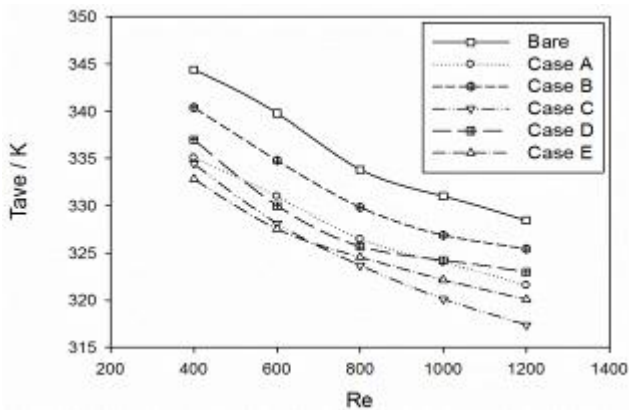


Fig. 4: Mean temperature versus Reynolds number at heat flux 100 W/cm²

3.4. Heat Transfer Characteristic

Nusselt number is used to verify the heat characteristic of different configuration of microchannel. The overall Nusselt number is calculated by:

$$Nu = hd / k_{fluid} \quad (3)$$

where k_{fluid} is the fluid thermal conductivity and h is the heat transfer coefficient which can be determined as:

$$h = \frac{Q}{NA_c \Delta T} \quad (4)$$

where Q is the total heat transfer, A_c is the contact surface area of fluid and solid wall and ΔT is the temperature gradient. Figure 5 plots the change of Nusselt number with different values of Reynolds number at heat flux of 100 W/m². As expected, the Nusselt number increased with the increasing Reynolds number in all cases. In particular, the Nusselt number in all five non-bare designs was higher than that of bare microchannel. The impact of Case C on the Nusselt number was similar to that caused by Case E, and much larger than those of Cases A, B and D. This could be attributed to the existence of semicircular and triangular ribs shrank the laminar stagnation zone which affects heat transfer of the microchannel. It is worth noting that Case E exhibited relative better performance at Reynolds number less than 700. However, a decline in performance can be seen with further increase of the Reynolds number. The variation of pressure drop factor with Reynolds number is shown in Figure 6.

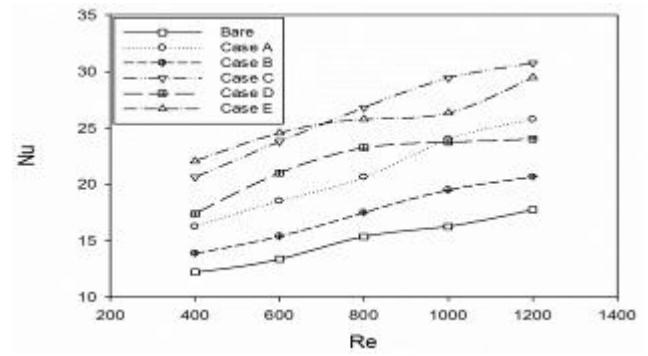


Fig. 5: Variation of Nusselt number with Reynolds number

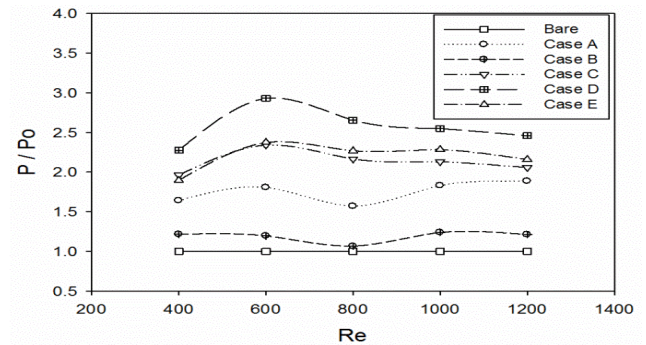


Fig. 6: Variation of pressure drop with Reynolds number

3.5. Overall Thermal Performance

Although the presence of extended surface improved the heat performance, however, the pressure loss also increased. Hence, the overall thermal performance should be calculated and compared with bare rectangular microchannel. The equation of thermal performance in this study can be derived as:

$$\eta = \frac{Nu / Nu_0}{(\Delta P / \Delta P_0)^{1/3}} \quad (5)$$

Figure 7 compares the overall thermal performance of all cases. As it can be clearly seen, the factor of overall thermal performance for all five cases was found to be greater than one (the bare microchannel). This proves that the extended surface in microchannel is important to improve the heat transfer performance of microchannels. An interesting phenomenon was noted that the thermal performance of case E was better than others before reaching the Reynolds number of 700. However, the performance deteriorates with Reynolds number greater than 700.

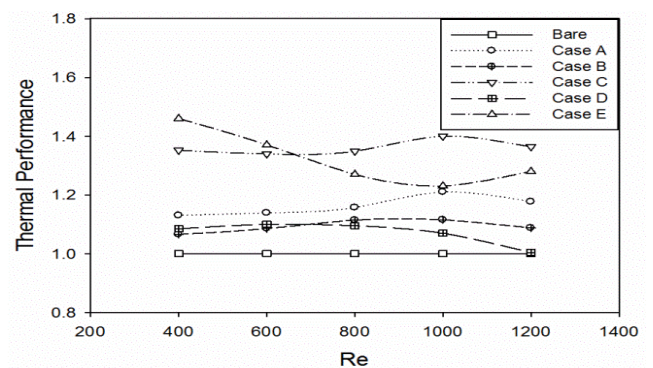


Fig. 7: Variation of overall thermal performance with Reynolds number

4. Conclusion

The flow structure and heat transfer in microchannel heat sink with microfins have been investigated numerically. Based on the findings, the Case E design can be employed at low Reynolds

number. On the other hand, the overall thermal performance of Case C is relatively better at higher Reynolds number, recording its peak at Reynolds number 1000. This is due to the fact that the diverging microfins in Case C with semicircular ribs provided the redevelopment of thermal boundary layer to enhance the heat transfer rate. The overall thermal performance of Case C is found to be 1.4 times greater than that of bare microchannel.

Acknowledgement

The project is funded by the University Internal Fund (UTARRF) under project IPSR/RMC/UTARRF/2016-C1/L1.

References

- [1] K.C. Lai, K.S. Ong, C.F. Tan, K.E. Ng, "Thermal field simulation of multi package LED module," in 4th International Symposium on Next-Generation Electronics, 2015, paper 7132012.
- [2] K.C. Lai, K.S. Ong, K.H. Tan, K.H. Yeap, M.H. Tan, "Thermal Simulation of Light-Emitting Diode Panel with Heat Sink," *Adv. Sci. Lett.*, 23(11), 11129–11133, 2017.
- [3] K.S. Ong, C.F. Tan, K.C. Lai, K.H. Tan, "Heat spreading and heat transfer coefficient with fin heat sink," *Appl. Therm. Eng.*, 112, 1638-1647, 2017.
- [4] A. Rezanian, L.A. Rosendahl, S.J. Andreasen, "Experimental investigation of thermoelectric power generation versus coolant pumping power in a microchannel heat sink," *Int. Commun. Heat Mass Transfer*, 39, 1054-1058, 2012.
- [5] K.S. Ong, C.F. Tan, K.C. Lai, "Methodological considerations of using thermoelectrics with fin heat sink for cooling applications," *Appl. Sci.*, 7(2), paper 62, 2017.
- [6] K.S. Ong, C.F. Tan, K.C. Lai, K.H. Tan, R. Singh, "Thermal management of LED with vapor chamber and thermoelectric cooling," in 37th IEEE International Electronics Manufacturing Technology Conference, 2016, paper 7761956.
- [7] K.S. Ong, P.L. Haw, K.C. Lai, K.H. Tan, "Vapor chamber with hollow condenser tube heat sink," *AIP Conference Proceedings*, 1828, paper 020018, 2017.
- [8] D. Deng, Y. Xie, Q. Huang, W. Wan, "On the flow boiling enhancement in interconnected reentrant microchannels," *Int. J. Heat Mass Transfer*, 108, 453-467, 2017.
- [9] I. Hassan, P. Phuttavong, M. Abdelgawad, "Microchannel heat sinks: An overview of the state-of-the-art," *Microscale Thermophysical Eng.*, 8, 183-205, 2004.
- [10] K. Vafai, L. Zhu, "Analysis of two-layered micro-channel heat sink concept in electronic cooling," *Int. J. Heat Mass Transfer*, 42, 2287-2297, 1999.
- [11] L.S. Maganti, P. Dhar, T. Sundararajan, S.K. Das, "Heat spreader with parallel microchannel configurations employing nanofluids for near-active cooling of MEMS," *Int. J. Heat Mass Transfer*, 111, 570-581, 2017.
- [12] T. Desrues, P. Marty, J. Fourmigué, "Numerical prediction of heat transfer and pressure drop in three-dimensional channels with alternated opposed ribs," *Appl. Therm. Eng.*, 45, 52–63, 2012.
- [13] S. Krishnamurthy, Y. Peles, "Flow boiling heat transfer on micro pin fins entrenched in a microchannel," *J. Heat Transfer*, 132, 041007, 2010.
- [14] Y.L. Zhai, G.D. Xia, X.F. Liu, Y.F. Li, "Heat transfer in the microchannels with fan-shaped reentrant cavities and different ribs based on field synergy principle and entropy generation analysis," *Int. J. Heat Mass Transfer*, 68, 224-233, 2014.
- [15] H.A. Mohammed, P. Gunnasegaran, N.H. Shuaib, "Numerical simulation of heat transfer enhancement in wavy microchannel heat sink," *Int. Commun. Heat Mass Transfer*, 38, 63-68, 2011.
- [16] Y.J. Cheng, "Numerical simulation of stacked microchannel heat sink with mixing-enhanced passive structure," *Int. Commun. Heat Mass Transfer*, 34, 295-303, 2007.
- [17] L. Chai, G. Xia, M. Zhou, J. Li, J. Qi, "Optimum thermal design of interrupted microchannel heat sink with rectangular ribs in the transverse microchambers," *Appl. Therm. Eng.*, 51, 880-889, 2013.
- [18] C.B. Zhang, Y.P. Chen, M.H. Shi, "Effects of roughness elements on laminar flow and heat transfer in microchannels," *Chem. Eng. Process.*, 49, 1188-1192, 2010.
- [19] V. Yadav, K. Baghel, R. Kumar, S.T. Kadam, "Numerical investigation of heat transfer in extended surface microchannels," *Int. J. Heat Mass Transfer*, 93, 612-622, 2016.
- [20] L. Chai, G. Xia, L. Wang, M. Zhou, Z. Cui, "Heat transfer enhancement in microchannel heat sinks with periodic expansion-constriction cross-sections," *Int. J. Heat Mass Transfer*, 62, 741-751, 2013.
- [21] M.E. Steinke, S.G. Kandlikar, "Single-phase liquid friction factors in microchannels," *Int. J. Therm. Sci.*, 45, 1073-1083, 2006.